

# Bayesian intrinsic groupwise registration via explicit hierarchical disentanglement

Xin Wang<sup>†,1,2</sup>, Xinzhe Luo<sup>†,1</sup>, and Xiahai Zhuang<sup>1</sup>

<sup>1</sup> School of Data Science, Fudan University, Shanghai, China

<sup>2</sup> Department of Electrical and Computer Engineering, University of Washington, Seattle, United States

**Abstract.** Previous methods on multimodal groupwise registration typically require certain highly specialized similarity metrics with restrained applicability. In this work, we instead propose a general framework which formulates groupwise registration as a procedure of hierarchical Bayesian inference. Here, the imaging process of multimodal medical images, including shape transition and appearance variation, is characterized by a disentangled variational auto-encoder. To this end, we propose a novel variational posterior and network architecture that facilitate joint learning of the common structural representation and the desired spatial correspondences. The performance of the proposed model was validated on two publicly available multimodal datasets, *i.e.*, BrainWeb and MS-CMR of the heart. Results have demonstrated the efficacy of our framework in realizing multimodal groupwise registration in an end-to-end fashion.

## 1 Introduction

Groupwise registration aims to achieve spatial alignment in a common structural space for images potentially from different modalities. It ameliorates the bias incurred by designating a reference image in pairwise registration, and thereby becomes an essential and fundamental task in multivariate image analysis, including longitudinal research, atlas generation, and population studies [8, 10, 13]. Conventional methods for multimodal groupwise registration usually rely on specially crafted intensity-based similarity measures [12, 16, 18, 25], the maximization of which is expected to produce the desired spatial correspondences. However, these measures often entail certain assumptions on the joint intensity profile, which can be violated in certain conditions [15].

Recently, unsupervised deep-learning methods are able to realize pairwise and groupwise registration in an end-to-end fashion [2, 4, 24]. Particularly in [4], the authors used the mutual information between warped images and a template image computed by principal component analysis (PCA) to train the network so that it could predict groupwise spatial correspondences. The metric is closely related to the conditional template entropy introduced in [18]. In summary, the success of learning-based registration can be mostly credited to the application of stochastic optimization with the existing similarity measures.

---

<sup>†</sup> The two authors contributed equally to this work.

In this paper, we instead shift attention from devising similarity metrics to learning disentangled representations of the imaging process. Specifically, a probabilistic generative model of the observed images is established, with spatial correspondences as part of the latent variables. Thus, groupwise registration is realized through unsupervised variational auto-encoding: the encoder infers groupwise spatial correspondences to the common structural codes by reversing the process of shape transition and appearance rendering, while the decoder learns to fit the imaging process and reconstructs the observed images.

The contributions of this work are summarized as follows: 1) We propose a theoretically grounded framework that formulates groupwise registration through Bayesian inference. 2) We propose a principled variational posterior to measure the intrinsic similarity over structural representations of multimodal images. 3) We propose a novel network architecture capable of disentangling from image appearances the structural codes that are equivariant to spatial transformations. 4) We demonstrate the effectiveness of our model on two multimodal image datasets and find superior performance to similarity-based learning methods. To the best of our knowledge, this is the first work that addresses multimodal groupwise registration using unsupervised disentanglement learning.

### 1.1 Related work

One particular work in the similar spirit as ours came from Qin et al. [19], where they used a complex disentanglement strategy comprising image translation, pairwise registration and adversarial similarity learning. Other relevant studies include [21, 22, 26]. These works mainly focused on natural images and can be used to deal with monomodal data. By contrast, our method is unified and principled, and is established purely from the theoretical interpretation of the disentangling nature with multimodal medical images.

## 2 Method

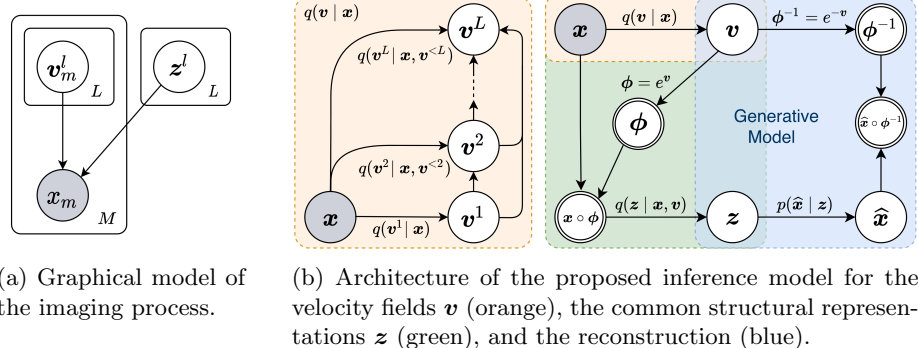
Groupwise registration aims to align multiple images into a common coordinate system  $\Omega$ . In this paper, we investigate particularly the case when the images are acquired from different modalities, denoted by  $\mathbf{X} = \{X_m\}_{m=1}^M$ , where  $X_m : \Omega_m \rightarrow \mathbb{R}$  reflects the imaging process and  $M$  is the number of modalities. Moreover, the images are assumed to be generated from a common structure  $\mathbf{S}$  combined with modality-specific appearance information  $\{\mathbf{A}_m\}_{m=1}^M$ , *i.e.*

$$X_m = f_m(\mathbf{S} \circ \phi_m^{-1}, \mathbf{A}_m), \quad (1)$$

where  $\phi = \{\phi_m : \Omega \rightarrow \Omega_m\}_{m=1}^M$  are the spatial transformations from the common space to the image spaces we seek to find.

### 2.1 Hierarchical Bayesian inference

We propose formalizing the estimation of groupwise spatial correspondences through Bayesian inference, as illustrated in Fig. 1. Specifically, let  $\mathbf{x} = (x_m)_{m=1}^M$



(a) Graphical model of the imaging process.

(b) Architecture of the proposed inference model for the velocity fields  $\mathbf{v}$  (orange), the common structural representations  $\mathbf{z}$  (green), and the reconstruction (blue).

Fig. 1: The proposed Bayesian framework. Random variables are in circles, deterministic variables are in double circles, and observed variables are shaded.

be a sample of the image group. We decompose the latent variables generating  $\mathbf{x}$  into two *independent* subgroups: 1) the latent representation  $\mathbf{z}$  that encodes the common structure  $\mathbf{S}$ , and 2) the stationary velocity fields  $\mathbf{v} = (\mathbf{v}_m)_{m=1}^M$  that parameterize the spatial transformations  $\phi = (\phi_m)_{m=1}^M$  [1]. Thus, the evidence lower bound (ELBO) of the log-likelihood takes the form

$$\mathcal{L}(\mathbf{x}) \triangleq \mathbb{E}_{q(\mathbf{z}, \mathbf{v} | \mathbf{x})} [\log p(\mathbf{x} | \mathbf{z}, \mathbf{v})] - D_{\text{KL}}[q(\mathbf{z}, \mathbf{v} | \mathbf{x}) \| p(\mathbf{z}) p(\mathbf{v})] \quad (2)$$

where  $q(\mathbf{z}, \mathbf{v} | \mathbf{x})$  defines the variational posterior distribution of the latent variables. Furthermore, the latent variables are expressed with hierarchical levels [23], *i.e.*  $\mathbf{z} = (\mathbf{z}^l)_{l=1}^L$ ,  $\mathbf{v} = (\mathbf{v}^l)_{l=1}^L$  and  $\mathbf{v}_m = (\mathbf{v}_m^l)_{l=1}^L$ , with  $L$  the number of levels and higher levels indicating finer-scale representations.

To simplify the term of the Kullback-Leibler (KL) divergence, we introduce additional independence assumptions: 1) both the prior and variational distributions of the velocity fields factorize with different images, *i.e.*  $p(\mathbf{v}^l | \mathbf{v}^{<l}) = \prod_{m=1}^M p(\mathbf{v}_m^l | \mathbf{v}_m^{<l})$  and  $q(\mathbf{v}^l | \mathbf{x}, \mathbf{v}^{<l}) = \prod_{m=1}^M q(\mathbf{v}_m^l | \mathbf{x}, \mathbf{v}_m^{<l})$ , and 2) the common structure  $\mathbf{z}^l$  at the  $l$ -th level can be inferred directly from the observed images and the estimated velocity fields, *i.e.*  $q(\mathbf{z}^l | \mathbf{x}, \mathbf{v}, \mathbf{z}^{<l}) = q(\mathbf{z}^l | \mathbf{x}, \mathbf{v})$ , where  $\mathbf{z}^{<l}$  are the structural representations up to the  $(l-1)$ -th level. The latter assumption is related to equivariance [5], which will be discussed in Section 2.3.

Taking into account these assumptions, the KL divergence can be written as

$$\begin{aligned} & D_{\text{KL}}[q(\mathbf{z}, \mathbf{v} | \mathbf{x}) \| p(\mathbf{z}) p(\mathbf{v})] \\ &= \sum_{m=1}^M \left[ \sum_{l=1}^L \mathbb{E}_{q(\mathbf{v}_m^l | \mathbf{x})} \left\{ D_{\text{KL}}[q(\mathbf{v}_m^l | \mathbf{x}, \mathbf{v}_m^{<l}) \| p(\mathbf{v}_m^l | \mathbf{v}_m^{<l})] \right\} \right] \quad (\text{i}) \quad (3) \\ &+ \mathbb{E}_{q(\mathbf{v} | \mathbf{x})} \left[ \sum_{l=1}^L \mathbb{E}_{q(\mathbf{z}^{<l} | \mathbf{x}, \mathbf{v})} \left\{ D_{\text{KL}}[q(\mathbf{z}^l | \mathbf{x}, \mathbf{v}) \| p(\mathbf{z}^l | \mathbf{z}^{<l})] \right\} \right] \quad (\text{ii}), \end{aligned}$$

where we define  $p(\mathbf{v}_m^1 | \mathbf{v}_m^{<1}) \triangleq p(\mathbf{v}_m^1)$ ,  $p(\mathbf{z}^1 | \mathbf{z}^{<1}) \triangleq p(\mathbf{z}^1)$  and  $q(\mathbf{v}_m^{<1} | \mathbf{x}) = q(\mathbf{z}^{<1} | \mathbf{x}, \mathbf{v}) \triangleq 1$ . Rigorous derivation of Eq. (3) can be found in the supple-

mentary material. Though intimidating at first glance, its idea is simple: the overall KL divergence in Eq. (3) is decomposed into terms *w.r.t.* (i) the velocity fields  $\mathbf{v}$ , and (ii) the common structure  $\mathbf{z}$ , following the proposed independence assumptions. The former serves as regularization for the velocity fields to ensure diffeomorphism, which is fulfilled by the constraint introduced in [7], with a hyper-parameter  $\lambda$  controlling its strength. The latter is intended to measure the similarity among the image group.

## 2.2 Intrinsic similarity over structural representations

To measure the intrinsic similarity over structural representations from multimodal images, we assume the joint variational posterior  $q(\mathbf{z}^l \mid \mathbf{x}, \mathbf{v})$  to be the geometric mean [14] while the joint prior  $p(\mathbf{z}^l \mid \mathbf{z}^{<l})$  to be the arithmetic mean [20] of the unimodal variational posteriors  $q_m(\mathbf{z}^l \mid \mathbf{x}_m, \mathbf{v}_m)$  that are predicted separately by the encoder for each modality, *i.e.*

$$q(\mathbf{z}^l \mid \mathbf{x}, \mathbf{v}) \triangleq \left[ \prod_{m=1}^M q_m(\mathbf{z}^l \mid \mathbf{x}_m, \mathbf{v}_m) \right]^{\frac{1}{M}}, \quad p(\mathbf{z}^l \mid \mathbf{z}^{<l}) \triangleq \frac{1}{M} \sum_{m=1}^M q_m(\mathbf{z}^l \mid \mathbf{x}_m, \mathbf{v}_m). \quad (4)$$

The unimodal posterior  $q_m(\mathbf{z}^l \mid \mathbf{x}_m, \mathbf{v}_m)$  is assumed to follow a factorized Gaussian distribution  $\mathcal{N}(\boldsymbol{\mu}_m^l, \boldsymbol{\Sigma}_m^l)$  and therefore so does the joint posterior, *i.e.*  $q(\mathbf{z}^l \mid \mathbf{x}, \mathbf{v}) = \mathcal{N}(\boldsymbol{\mu}^l, \boldsymbol{\Sigma}^l)$  with

$$\boldsymbol{\Sigma}^l = M \cdot \left[ \sum_{m=1}^M (\boldsymbol{\Sigma}_m^l)^{-1} \right]^{-1}, \quad \boldsymbol{\mu}^l = \frac{\boldsymbol{\Sigma}^l}{M} \cdot \sum_{m=1}^M \boldsymbol{\mu}_m^l (\boldsymbol{\Sigma}_m^l)^{-1}. \quad (5)$$

In light of the computational intractability involving Gaussian mixture distributions, we further exploit the convexity of KL divergence to obtain

$$D_{\text{KL}}[q(\mathbf{z}^l \mid \mathbf{x}, \mathbf{v}) \parallel p(\mathbf{z}^l \mid \mathbf{z}^{<l})] \leq \frac{1}{M} \sum_{m=1}^M D_{\text{KL}}[q(\mathbf{z}^l \mid \mathbf{x}, \mathbf{v}) \parallel q_m(\mathbf{z}^l \mid \mathbf{x}_m, \mathbf{v}_m)]. \quad (6)$$

Hence, minimizing the right-hand side of Eq. (6) encourages the unimodal posteriors to be identical, thus forcing the variational distributions to represent modality-invariant structures located in the common space.

## 2.3 Explicit disentanglement with neural networks

We propose a dedicated hierarchical variational auto-encoder (VAE) as the inference model in Fig. 1(b) to maximize the ELBO. An example of the network architecture with the number of hierarchy  $L = 3$  is depicted in Fig. 2.

The essence of the network is its capability to explicitly disentangle the common structure, spatial transformations and appearance information in Eq. (1) from multimodal images. To this end, the network is decomposed into three types

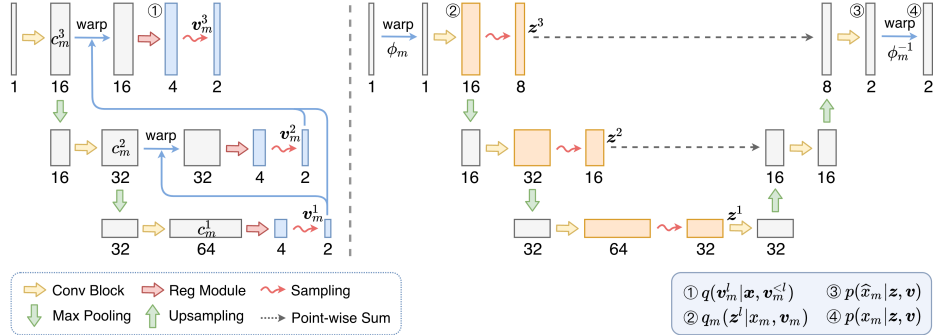


Fig. 2: Network architecture ( $L = 3$ ) for explicit disentanglement. The features in blue indicate  $q(\mathbf{v}_m^l)$  and the sampled  $\mathbf{v}_m^l$ , while those in orange indicate  $q_m(\mathbf{z}^l)$  and the latent representations sampled from the joint variational posterior  $q(\mathbf{z}^l)$ . Except for  $\mathbf{z}^l$ , the channel number below each feature is specific to one modality.

of submodules: 1) an encoder that extracts modality-invariant structural codes, 2) multi-level registration (Reg) modules that infer spatial transformations from the structural codes, and 3) a decoder, with modality-specific appearance information embedded, reconstructing original images from the learned common structure and the inverse mappings to the image spaces.

**Bottom-up inference of velocity fields.** To learn the velocity fields that co-register the image group, the encoder first infers multilevel structural codes  $\mathbf{c}_m^l(x_m) \triangleq [\tilde{\mu}_m^l(x_m); \ln \tilde{\Sigma}_m^l(x_m)]$  from each modality. Note that these structural codes are assumed to be located in the corresponding image spaces. They are associated with the unimodal variational posteriors via equivariance, *i.e.*

$$\mathbf{c}_m^l(x_m \circ \phi_m) = [\tilde{\mu}_m^l(x_m) \circ \phi_m; \ln \tilde{\Sigma}_m^l(x_m) \circ \phi_m] = [\mu_m^l; \ln \Sigma_m^l], \quad \forall \phi_m. \quad (7)$$

Then, up from the bottom of the encoder, the registration module at level  $l$  infers the parameters of  $q(\mathbf{v}_m^l | \mathbf{x}, \mathbf{v}_m^{<l})$  based on the concatenation of  $\tilde{\mu}_m^l \circ \phi_m^{<l}$  and the average of  $(\tilde{\mu}_m^l \circ \phi_m^{<l})_{m=1}^M$  weighted by the variances  $(\tilde{\Sigma}_m^l \circ \phi_m^{<l})_{m=1}^M$  using Eq. (5), where  $\phi_m^{<l} \triangleq \phi_m^1 \circ \dots \circ \phi_m^{l-1}$ . Thus, the velocity field  $\mathbf{v}_m^l$  is sampled from the variational posterior  $q(\mathbf{v}_m^l | \mathbf{x}, \mathbf{v}_m^{<l})$ .

**Top-down inference of common structures.** To infer the common structural information, the encoder is fed with the warped images  $\mathbf{x} \circ \phi \triangleq (x_m \circ \phi_m)_{m=1}^M$  using the sampled velocity fields and produces the unimodal variational posteriors  $q_m(\mathbf{z}^l | x_m, \mathbf{v}_m)$  down from the top for  $m = 1, \dots, M$  separately. The latent variable  $\mathbf{z}^l$  of the common structure is then sampled from the joint posterior  $q(\mathbf{z}^l | \mathbf{x}, \mathbf{v})$  computed by Eq. (4).

**Disentangled auto-encoding.** To attain a better disentanglement of structure and appearance, we further leverage the strategy that the convolutional layers of the auto-encoder are shared across modalities, while domain-specific batch normalization layers (BNs) encodes the appearance information for each modality [3]. Thus, the encoder extracts modality-invariant common structure

$\mathbf{z}$ , based on which the decoder estimates the distributions of the registered images  $\widehat{\mathbf{x}} = (\widehat{x}_m)_{m=1}^M$  in the common space, and then reconstructs the distributions of the original images by inverse spatial transformations, whereby  $p(\mathbf{x} | \mathbf{z}, \mathbf{v}) = p(\widehat{\mathbf{x}} \circ \phi^{-1} | \mathbf{z}, \mathbf{v})$ , with  $\widehat{\mathbf{x}} \circ \phi^{-1} \triangleq (\widehat{x}_m \circ \phi_m^{-1})_{m=1}^M$ .

### 3 Experiments and Results

#### 3.1 Datasets

Experiments were conducted on two public multimodal image datasets.

**BrainWeb.** The dataset comprises three sequences of brain magnetic resonance (MR) volumes, namely T1, T2 and proton-density (PD) weighted, which were synthesized from an MR image simulator and thereby well aligned [6]. The images were skull-stripped and then sequentially deteriorated by noise and intensity non-uniformity to simulate real imaging conditions. One designated slice was repeatedly contorted by synthetic free-form deformations (FFDs), to generate image groups with four different degrees of distortion. Particularly, 40 groups were randomly selected for training, 40 for validation, and 80 for test. During training, distorted images were combined among sequences with the same distortion degree, resulting in a total of  $10^3 \times 4 = 4000$  training groups.

**MS-CMR.** The MS-CMRSeg challenge [27,28] provided multi-sequence cardiac MR images from 45 patients. The sequences include LGE, bFFSP and T2, which exhibit complementary information of the cardiac structure. The images were preprocessed by affine co-registration, ROI cropping and slice selection. A total of 39 slices were used for training, 15 for validation and 44 for test. The sequences were pre-aligned, thus we imposed synthetic FFDs on the original images to better demonstrate the efficacy of the proposed registration method.

#### 3.2 Experimental setups

**Registration methods.** Two groupwise registration methods were compared on both datasets: 1) the proposed model that integrates groupwise registration with disentangled representation learning, 2) a similarity-based learning method that stochastically optimizes the accumulated pairwise estimates (APE) using a residual U-Net (ResUNet) as the backbone [9] and mutual information as the similarity metric [25].

**Implementation details.** During preprocessing, we performed min-max normalization for each image. For network structure, each convolutional block, denoted by  $C_k$ , comprises  $k$  sub-blocks of Conv-BN-LeakyReLU. We set  $k = 2$  for both the encoder and decoder, while each Reg module consists of a  $C_m$  plus a Conv. Besides, each upsampling involves a bilinear scaling followed by a Conv to adjust the channel number. To better balance registration and reconstruction, we adopted  $1 \times 1$  Convs in the decoder, and  $3 \times 3$  Convs in the rest of the network. We also set the momentum of all BNs to 0.01 to boost generalizability. The training took 500 epochs through the Adam optimizer [11] with a learning

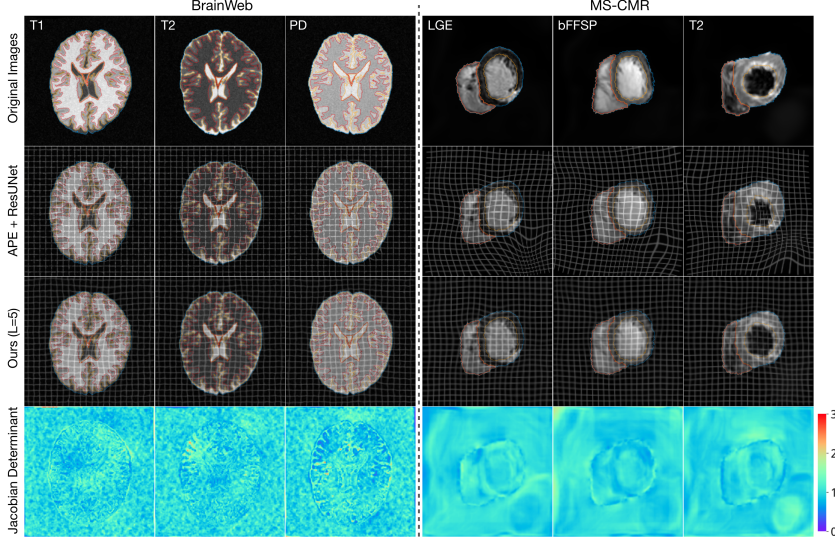


Fig. 3: Example image groups, with segmentation contours overlaid, from the two datasets before and after registration using different methods, and the Jacobian determinants of the deformations predicted by the proposed model.

rate of  $10^{-3}$  and a batch size of 20. The experiments were conducted on an NVIDIA® RTX™ 3090 GPU and the code was implemented in PyTorch [17].

**Evaluation metrics.** For the BrainWeb dataset, as the images were distorted by initial misalignments  $\phi^\dagger = (\phi_m^\dagger)_{m=1}^M$  and then co-registered, we use the groupwise warping index (gWI) as an evaluation metric, namely

$$gWI(\phi^\dagger, \hat{\phi}) = \frac{1}{M} \sum_{m=1}^M \sqrt{\frac{1}{|\hat{\Omega}_m^f|} \sum_{\omega \in \hat{\Omega}_m^f} \|\bar{r}_m(\omega)\|_2^2}, \quad (8)$$

where  $\hat{\phi} = (\hat{\phi}_m)_{m=1}^M$  are the estimated groupwise spatial correspondences,  $\hat{\Omega}_m^f \triangleq \{\omega \in \Omega \mid \phi_m^\dagger \circ \hat{\phi}_m(\omega) \in F\}$  with  $F$  the foreground region of the initial phantom,  $\bar{r}_m(\omega) \triangleq r_m(\omega) - \frac{1}{M} \sum_{m'} r_{m'}(\omega)$  and  $r_m(\omega) \triangleq \phi_m^\dagger \circ \hat{\phi}_m(\omega) - \omega$ . The gWI will reduce to zero if the initial misalignments are perfectly recovered. Besides, we reported for both datasets the average Dice similarity coefficient (DSC) calculated from all pairs of propagated segmentation masks with the registered images.

### 3.3 Results

The quantitative metrics evaluated on the test sets are summarized in Table 1. We herein reported the performance of the proposed model with different numbers of hierarchy, namely  $L = 4$  or  $5$ . For fair comparisons, the number of convolutional blocks in the encoder of the ResUNet was also set to 5. In terms of

Table 1: Test results on the BrainWeb and MS-CMR datasets. The table presents the mean values and standard deviations of the gWI (in millimeters) and DSC before and after groupwise registration using different methods.

| Method           | BrainWeb                            |                                     | MS-CMR                              |
|------------------|-------------------------------------|-------------------------------------|-------------------------------------|
|                  | DSC $\uparrow$                      | gWI (mm) $\downarrow$               | DSC $\uparrow$                      |
| None             | $0.668 \pm 0.141$                   | $2.424 \pm 1.784$                   | $0.722 \pm 0.101$                   |
| APE + ResUNet    | $0.834 \pm 0.039$                   | $1.789 \pm 1.218$                   | $0.777 \pm 0.040$                   |
| Ours ( $L = 4$ ) | $0.863 \pm 0.021$                   | $1.007 \pm 0.743$                   | $0.841 \pm 0.050$                   |
| Ours ( $L = 5$ ) | <b><math>0.873 \pm 0.009</math></b> | <b><math>0.716 \pm 0.385</math></b> | <b><math>0.870 \pm 0.044</math></b> |

the Dice coefficient and gWI, our method significantly surpasses the similarity-based method ( $p \ll 0.001$ ). The latter metric, in particular, demonstrates that our model can yield a more accurate groupwise alignment in the common space. In addition, our network performance is enhanced with a higher  $L$ , which shows the superiority of our hierarchical decomposition strategy for the latent variables.

The registration results of the investigated methods are visualized in Fig. 3, including the image groups before and after registration, together with the corresponding segmentation masks, estimated deformations and Jacobian determinants. It is evident that the proposed method achieves better spatial correspondence for both large-scale anatomy and local fine structures, compared with the similarity-based method. The estimated deformations also reach great smoothness and diffeomorphism, indicated by the determinant values.

## 4 Conclusion

In this paper, we proposed an elegant Bayesian framework for unsupervised multimodal groupwise registration. To avoid the reliance on carefully-designed similarity metrics, we presented a principled variational posterior to learn the structural representations, and built a dedicated architecture for the estimation of such intrinsic similarity through hierarchical disentanglement of the common structure, image appearance, and spatial transformations. Results on two public multimodal datasets demonstrated the superior performance of our model compared to similarity-based approaches.

Based on the well-disentangled appearance and structural representations embedded in the network, our model possesses great interpretability, and has the potential for other applications, such as multimodal segmentation and image fusion. Future work includes exploration of such potential and extensions of the variational framework to more applications.

## References

1. Ashburner, J.: A fast diffeomorphic image registration algorithm. *Neuroimage* **38**(1), 95–113 (2007)
2. Balakrishnan, G., Zhao, A., Sabuncu, M.R., Guttag, J., Dalca, A.V.: Voxelmorph: a learning framework for deformable medical image registration. *IEEE transactions on medical imaging* **38**(8), 1788–1800 (2019)
3. Chang, W.G., You, T., Seo, S., Kwak, S., Han, B.: Domain-specific batch normalization for unsupervised domain adaptation. In: *Proceedings of the IEEE/CVF Conference on Computer Vision and Pattern Recognition*. pp. 7354–7362 (2019)
4. Che, T., Zheng, Y., Sui, X., Jiang, Y., Cong, J., Jiao, W., Zhao, B.: Dgr-net: Deep groupwise registration of multispectral images. In: *International Conference on Information Processing in Medical Imaging*. pp. 706–717. Springer (2019)
5. Cohen, T., Welling, M.: Group equivariant convolutional networks. In: *International conference on machine learning*. pp. 2990–2999. PMLR (2016)
6. Collins, D., Zijdenbos, A., Kollokian, V., Sled, J., Kabani, N., Holmes, C., Evans, A.: Design and construction of a realistic digital brain phantom. *IEEE Transactions on Medical Imaging* **17**(3), 463–468 (1998)
7. Dalca, A.V., Balakrishnan, G., Guttag, J., Sabuncu, M.R.: Unsupervised learning of probabilistic diffeomorphic registration for images and surfaces. *Medical image analysis* **57**, 226–236 (2019)
8. Geng, X., Christensen, G.E., Gu, H., Ross, T.J., Yang, Y.: Implicit reference-based group-wise image registration and its application to structural and functional MRI. *Neuroimage* **47**(4), 1341–1351 (Oct 2009)
9. Hu, Y., Modat, M., Gibson, E., Li, W., Ghavami, N., Bonmati, E., Wang, G., Bandula, S., Moore, C.M., Emberton, M., et al.: Weakly-supervised convolutional neural networks for multimodal image registration. *Medical image analysis* **49**, 1–13 (2018)
10. Joshi, S.C., Davis, B.C., Jomier, M., Gerig, G.: Unbiased diffeomorphic atlas construction for computational anatomy. *NeuroImage* **23**, S151–S160 (2004)
11. Kingma, D.P., Ba, J.: Adam: A method for stochastic optimization. In: Bengio, Y., LeCun, Y. (eds.) *3rd International Conference on Learning Representations, ICLR 2015, San Diego, CA, USA, May 7-9, 2015, Conference Track Proceedings* (2015)
12. Learned-Miller, E.G.: Data driven image models through continuous joint alignment. *IEEE Transactions on Pattern Analysis and Machine Intelligence* **28**(2), 236–250 (2005)
13. Liao, S., Jia, H., Wu, G., Shen, D.: A novel framework for longitudinal atlas construction with groupwise registration of subject image sequences. *Neuroimage* **59**(2), 1275–1289 (Jan 2012)
14. Lorenzen, P., Prastawa, M., Davis, B., Gerig, G., Bullitt, E., Joshi, S.: Multi-modal image set registration and atlas formation. *Medical image analysis* **10**(3), 440–451 (2006)
15. Luo, X., Zhuang, X.: Mvmm-regnet: A new image registration framework based on multivariate mixture model and neural network estimation. In: *International Conference on Medical Image Computing and Computer-Assisted Intervention*. pp. 149–159. Springer (2020)
16. Orchard, J., Mann, R.: Registering a multisensor ensemble of images. *IEEE Transactions on Image Processing* **19**(5), 1236–1247 (2009)

17. Paszke, A., Gross, S., Chintala, S., Chanan, G., Yang, E., DeVito, Z., Lin, Z., Desmaison, A., Antiga, L., Lerer, A.: Automatic differentiation in pytorch (2017)
18. Polfliet, M., Klein, S., Huizinga, W., Paulides, M.M., Niessen, W.J., Vandemeulebroucke, J.: Intrasubject multimodal groupwise registration with the conditional template entropy. *Medical image analysis* **46**, 15–25 (2018)
19. Qin, C., Shi, B., Liao, R., Mansi, T., Rueckert, D., Kamen, A.: Unsupervised deformable registration for multi-modal images via disentangled representations. In: International Conference on Information Processing in Medical Imaging. pp. 249–261. Springer (2019)
20. Shi, Y., Paige, B., Torr, P., et al.: Variational mixture-of-experts autoencoders for multi-modal deep generative models. *Advances in Neural Information Processing Systems* **32**, 15718–15729 (2019)
21. Shu, Z., Sahasrabudhe, M., Guler, R.A., Samaras, D., Paragios, N., Kokkinos, I.: Deforming autoencoders: Unsupervised disentangling of shape and appearance. In: Proceedings of the European conference on computer vision (ECCV). pp. 650–665 (2018)
22. Skafte, N., Hauberg, S.: Explicit disentanglement of appearance and perspective in generative models. *Advances in Neural Information Processing Systems* **32**, 1018–1028 (2019)
23. Vahdat, A., Kautz, J.: Nvae: A deep hierarchical variational autoencoder. *arXiv preprint arXiv:2007.03898* (2020)
24. de Vos, B.D., Berendsen, F.F., Viergever, M.A., Sokooti, H., Staring, M., Işgum, I.: A deep learning framework for unsupervised affine and deformable image registration. *Medical image analysis* **52**, 128–143 (2019)
25. Wachinger, C., Navab, N.: Simultaneous registration of multiple images: Similarity metrics and efficient optimization. *IEEE transactions on pattern analysis and machine intelligence* **35**(5), 1221–1233 (2012)
26. Xing, X., Gao, R., Han, T., Zhu, S.C., Wu, Y.N.: Deformable generator networks: Unsupervised disentanglement of appearance and geometry. *IEEE Transactions on Pattern Analysis and Machine Intelligence* (2020)
27. Zhuang, X.: Multivariate mixture model for myocardial segmentation combining multi-source images. *IEEE transactions on pattern analysis and machine intelligence* **41**(12), 2933–2946 (2019)
28. Zhuang, X., Xu, J., Luo, X., Chen, C., Ouyang, C., Rueckert, D., Campello, V.M., Lekadir, K., Vesal, S., RaviKumar, N., et al.: Cardiac segmentation on late gadolinium enhancement mri: a benchmark study from multi-sequence cardiac mr segmentation challenge. *arXiv preprint arXiv:2006.12434* (2020)